Task-Oriented Workspace Analysis and Operating Plane Selection of a 3-RSR Parallel Haptic Interface

Alessandro Genua, Eleonora Storto, Francesco Porcini, Massimiliano Solazzi, and Antonio Frisoli

Abstract Assessing the workspace and orientation capabilities of parallel manipulators is a classical problem in robot kinematics, but it becomes particularly challenging in *task-dependent variable workspace* scenarios, where the operating region depends on the specific task. This work addresses such a case in teleultrasound, focusing on a parallel mechanism conceived as a leader interface generating probe-like motions. The aims of this study are threefold: (i) to establish a compatibility-based kinematic framework linking screw-theoretic constraints with numerical inverse kinematics, (ii) to introduce task-oriented performance metrics combining translational conditioning and orientation regularity, and (iii) to define a criterion for identifying a task-dependent *operating plane* z^* where the leader mechanism exhibits favorable kinematic behavior. The proposed methodology is applied to a custom 3-RSR parallel mechanism. The inverse kinematics is formulated through compatibility equations and solved via a nonlinear least-squares approach, while the Jacobian is validated for consistency with the kinematic constraints. For numerical evaluation, the configuration space is parametrized in Cartesian coordinates and discretized into horizontal slices, each analyzed in terms of conditioning and orientation smoothness. These indices are combined into a composite score that highlights a preferred operating plane. The results confirm the suitability of the 3-RSR

A. Genua
Scuola Superiore Sant'Anna Pisa, Pisa, Italy
e-mail: `alessandro.genua@santannapisa.it`

E. Storto
Scuola Superiore Sant'Anna Pisa, Pisa, Italy

F. Porcini
Scuola Superiore Sant'Anna Pisa, Pisa, Italy

M. Solazzi
Scuola Superiore Sant'Anna Pisa, Pisa, Italy

A. Frisoli
Scuola Superiore Sant'Anna Pisa, Pisa, Italy

architecture as a leader interface for teleoperation tasks and demonstrate how the proposed framework provides a systematic way to identify task-oriented operating regions. Although illustrated with an ultrasound-related scenario, the approach is general and can be extended to other teleoperation or manipulation contexts.

1 Introduction

Workspace analysis is a classical problem in robotic design and is commonly used to compare kinematic structures in terms of extent and shape [7]. When task-oriented requirements must be satisfied, however, geometric reachability alone is insufficient, and the quality and regularity of the attainable motions become equally important, particularly in teleoperation scenarios where predictability and smoothness directly affect usability. Teleultrasound is a representative example of task-oriented teleoperation, enabling remote diagnostic services in real time [2, 13]. Recent reviews highlight how the architecture of leaderfollower systems and the design of the human interface critically affect the interactions [14]. Teleultrasound systems are composed of a leader site in which the clinician, through an interface device, controls the motion of a real probe located at the end-effector of a robot at the follower site, where the patient is located. During a conventional examination, the physician combines gross positioning with finer probe movements (including linear translations along the patients body, pitch and yaw rotations around a fixed point, and axial rotations along the probes longitudinal axis [11]) to acquire clinically relevant imaging planes while maintaining contact with the patients body. Parallel manipulators are widely used as leader interfaces due to their favorable kinematic properties [10, 15]. Several studies have investigated the task-oriented design and optimization of parallel structures for haptic interfaces, where the mechanism geometry is tuned to match the desired workspace and motion characteristics [1].

The 3-RSR parallel manipulator provides a suitable basis for teleultrasound applications, as its roto-translational motion naturally conforms to the anatomical curvatures of the human body. This capability facilitates the identification and tracking of optimal ultrasound imaging planes. To allow the clinician to reproduce the full set of probe motions, the end-effector is complemented with a passive spherical wrist. 3-RSR screw-theoretic formulation and constraint structure [3, 4], provide a solid foundation for compatibility-based approaches. This paper addresses this gap by introducing a compatibility-based kinematic framework for the analysis of the operating region of a 3-RSR parallel leader interface. The configuration space is parametrized in Cartesian coordinates and discretized into horizontal slices, evaluated in terms of translational Jacobian conditioning and orientation regularity. From these metrics, a task-dependent *operating plane* z^* is identified, corresponding to a region where the leader exhibits well-conditioned behavior. In a leader–follower setup, anchoring the leader at z^* enables predictable orientation behavior, while the follower adapts its motion accordingly. The main contributions are: (I) a compatibility-based kinematic framework for task-oriented analysis of parallel leader interfaces in teleoperation, (II) a composite metric combining translational conditioning and orientation regularity, and (III) the definition of a task-dependent operating plane linking kinematic behavior to teleoperation requirements.

The remainder of the paper is organized as follows: Section 2 presents the methodology, Section 3 reports the numerical results, and Section 4 discusses the main findings and future directions.

2 Methodology and Case Study

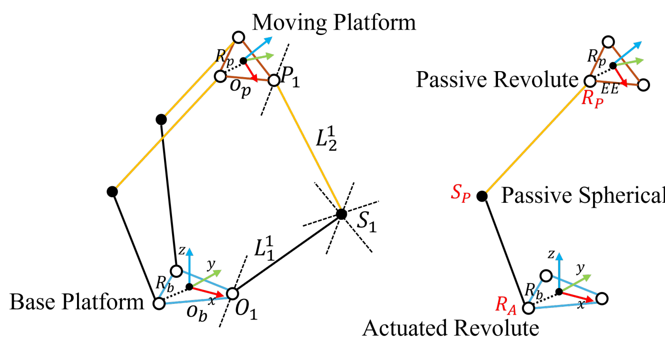

Fig. 1 Kinematic structure of the 3-RSR parallel manipulator. The actuated revolute joint R_A, the spherical joint S_P, and the passive revolute joint R_P connecting the moving platform are illustrated together with the local reference frames.

2.1 Mechanism architecture and inverse kinematics

The symmetric 3-RSR parallel architecture is composed of three identical kinematic chains (Fig. 1) that connects the fixed base to the moving platform through an actuated revolute joint R_A, a spherical joint S_P, and a passive revolute joint R_P. The actuated joints are arranged at the vertices of an equilateral triangle with in-plane axes spaced by 120°, with the same arrangement on the moving platform. According to the type synthesis of [7] and the kinematic analysis of [4], the symmetric 3-RSR architecture admits three independent degrees of freedom (DoFs), corresponding to the relative separation between the base and the moving platform and to platform tilting about two horizontal directions. As such, the mechanism does not provide independent translational and rotational motions in Cartesian space, but operates on a three-dimensional kinematic manifold. The reference geometry adopts link lengths

$L_1 = 300$ mm and $L_2 = 380$ mm, with base and moving platform radii $R_b = 100$ mm and $R_p = 60$ mm, respectively.

The presence of the intermediate spherical joint prevents a closed-form solution of the inverse kinematics. Numerical solvers based on geometric and kinematic constraints are therefore required [8]. Inverse kinematics is formulated using screw-theoretic compatibility equations and solved numerically via a nonlinear least-squares algorithm Levenberg–Marquardt (LM), initialized with geometrically consistent guesses. The numerical problem is formulated as the minimization of the residual vector $F(\mathbf{x})$, where $\mathbf{x} = [\alpha, \beta, \gamma, q_1, q_2, q_3]^T$ collects the platform orientation parameters and the actuated joint angles. For each leg i, two compatibility conditions are enforced: (i) the distance constraint $\|P_i - S_i\| - L_2 = 0$, and (ii) the orthogonality condition $v_i \cdot (S_i - P_i) = 0$ between the passive revolute axis v_i and the corresponding link direction. The solver therefore minimizes $\min \|F(\mathbf{x})\|^2$ using a LM scheme. Multiple initial guesses are generated around the neutral configuration to improve robustness of convergence. The solver returns both actuated joint angles and passive joint configurations for each admissible pose. Joint limits from the CAD geometry (e.g., -3° to 60° for the actuated joints) are enforced to ensure physically admissible configurations and avoid mechanical interference between links and joints. They were obtained from the geometric model of the mechanism considering both link interference and the motion ranges of commercial spherical joints used as design references. Convergence is reached when the residual norm falls below 10^{-8}. Within the explored workspace sampling, the solver converged successfully for more than 95% of the tested configurations. The inverse kinematics is solved via a multi-start nonlinear least-squares scheme, each solve involves six variables, the computational cost is moderate for the considered offline analysis.

2.2 Jacobian derivation and workspace sampling procedure

Following screw theory, the instantaneous motion of the moving platform is described by a twist \$ expressed in Plücker coordinates. Each kinematic chain transmits a set of reciprocal constraint wrenches associated with its passive joints, which restrict the admissible platform motion. The compatibility conditions therefore enforce that the platform twist belongs to the subspace spanned by the actuation screws while remaining reciprocal to all constraint wrenches imposed by the mechanism. Kinematic constraints of each chain are expressed in screw form following the formulation of Di Gregorio [4]. For the i-th leg, the closure condition relates the platform twist \$ and the actuated joint rate $\dot{q}_i$ through the compatibility relation $A_i \$ = B_i \dot{q}_i$, where A_i collects the reciprocal constraint wrenches transmitted by the leg and B_i maps the joint rate into the corresponding actuation screw. By stacking the three kinematic chains, the global constraint system is obtained as $A \$ = B \dot{\mathbf{q}}$ together with $C \$ = 0$, where A is the actuation wrench matrix, B the actuation matrix, and C the matrix collecting all reciprocal constraint wrenches associated with passive joints. The manipulator Jacobian J is then obtained by enforcing the relation

$\$ = J\dot{\mathbf{q}}$ while satisfying the compatibility conditions $AJ = B$ and $CJ = 0$, ensuring that the resulting platform twist is consistent with both actuation and constraint screws. The geometric Jacobian $J \in \mathbb{R}^{6\times 3}$ maps the three actuated joint velocities to the platform twist, with the admissible motion restricted to the three-dimensional kinematic manifold defined by the mechanism constraints. The configuration space is parametrized in Cartesian coordinates as a numerical embedding of the admissible kinematic manifold, rather than as a representation of independent Cartesian DoF, and is discretized along the z axis. For each slice, the (x,y) plane is sampled on a uniform 41×41 grid with 5 mm spacing over a 200×200 mm region. With $N_z = 9$ slices, a total of 15,129 candidate configurations are evaluated, consistent with established numerical workspace exploration methods [12]. The 5 mm grid spacing was selected to ensure that angular changes between adjacent points remain well below the regularity threshold τ. At each grid point, inverse kinematics is solved. The Jacobian is computed and validated, and the following kinematic indices are stored: (I) translational conditioning, computed from the Jacobian block $J_t = J(1{:}3,:)$; (II) orientation gradients of yaw, pitch, and roll. Numerical inverse kinematics solutions are retained only if the residuals $\|AJ - B\|$ and $\|CJ\|$ fall below a tolerance of 10^{-8}, guaranteeing consistency between numerical results and the underlying screw-theoretic model.

2.3 Performance metrics and composite-score

Each z-slice of the operating region is evaluated using the following metrics.

Reachability: For a given slice $z = z_k$, (k-th discretized slice of the configuration space along the vertical direction), reachability is defined as the percentage of grid points yielding valid inverse kinematics solutions:

$$\mathrm{Reach}(z_k) = \frac{\left\{(x,y) : \text{IK valid and } {}^{\|AJ-B\|<\varepsilon}_{\|CJ\|<\varepsilon}\right\}}{\{(x,y)\}} \times 100\%. \tag{1}$$

This definition is consistent with prior workspace analysis [6].

Orientation Regularity: Platform orientation is reconstructed using Euler angles $(\mathrm{yaw}, \mathrm{pitch}, \mathrm{roll})$. Spatial gradients are computed on the grid, and orientation regularity is quantified as: $G(z_k) = \frac{1}{3}\left(\mathrm{median}(\|\nabla Y\|) + \mathrm{median}(\|\nabla P\|) + \mathrm{median}(\|\nabla R\|)\right)$.

The spatial gradients are computed as the magnitude of the planar derivatives of the Euler angles. For a generic orientation component $\theta \in \{Y,P,R\}$ (yaw, pitch, roll), the gradient magnitude is defined as: $\|\nabla\theta\| = \sqrt{(\partial\theta/\partial x)^2 + (\partial\theta/\partial y)^2}$. The derivatives are evaluated numerically on the discretized grid using finite differences. Central differences are used for interior grid points, while first-order forward/backward differences are used at the slice boundaries. Orientation gradients are expressed in radians per millimeter (rad/mm).

A "regular area" percentage is also computed as the fraction of cells satisfying $\|\nabla P\| < \tau$, with $\tau = 8.73 \times 10^{-4}\,\mathrm{rad/mm}$ (equivalent to $0.05^\circ/\mathrm{mm}$) [9]. The heuristic threshold τ was selected to identify regions where orientation changes remain very small over the spatial resolution of the sampling grid (5 mm). This corresponds to an angular variation of approximately 0.25° between adjacent grid points, representing a sufficiently smooth tilting motion for probe-like teleoperation.

Translational Conditioning: From the geometric Jacobian $J \in \mathbb{R}^{6\times 3}$, the translational block $J_t \in \mathbb{R}^{3\times 3}$ is extracted and evaluated as: $C(z_k) = \mathrm{median}_{(x,y)}\left[\log_{10}\kappa(J_t)\right]$ where $\kappa(\cdot)$ denotes the condition number, commonly used to assess kinematic robustness [5, 16]. Since J_t relates joint velocities to linear platform velocities only, the resulting matrix is dimensionally homogeneous and avoids the unit inconsistency that may arise when translational and rotational components are combined in the full Jacobian.

Slice comparison is based on a composite score combining translational conditioning and orientation regularity. Both metrics are normalized to $[0,1]$:

$$\tilde{C}(z) = \frac{C(z) - \min C}{\max C - \min C}, \qquad \tilde{G}(z) = \frac{|G(z) - G_{\mathrm{target}}|}{\max_k |G(z_k) - G_{\mathrm{target}}|}.$$

The composite score is: $S(z) = w_g\,\tilde{G}(z) + w_c\,\tilde{C}(z)$; and the operating plane z^* is selected as the minimizer of $S(z)$, with ties resolved by maximizing the fraction of regular cells. The weights w_g and w_c reflect the relative importance of orientation regularity and translational conditioning for the considered task. In teleultrasound-inspired manipulation, smooth probe tilting is a primary requirement for image stability, and orientation regularity was therefore given slightly higher importance. For this reason the weights were selected as $w_g = 0.6$ and $w_c = 0.4$. Since both metrics are normalized, moderate variations of the weights are not expected to significantly affect the identification of the optimal operating plane.

The plane z^* is the task-dependent configuration where kinematic controllability and orientation regularity are jointly optimized, enabling predictable probe-like motions in the leader–follower architecture. Although demonstrated in a teleultrasound-inspired scenario, the same selection logic applies to other task-oriented teleoperation or manipulation problems by appropriately tuning G_{target}. The parameter G_{target} represents the expected probe tilting gradient for a given anatomical surface, with different values corresponding to regions of different curvature radii.

3 Results

Inverse kinematics shows nearly 100% reachability across all analyzed z-slices within the sampled 200×200 mm region, indicating that admissible configurations exist for almost all grid points. Orientation behavior is assessed through the spatial gradients of the Euler angles. Fig. 2 reports the median gradients of yaw, pitch, and roll as functions of the height z. For the considered teleoperation task, pitch variations are the most relevant component of the probe-like motion. The spatial

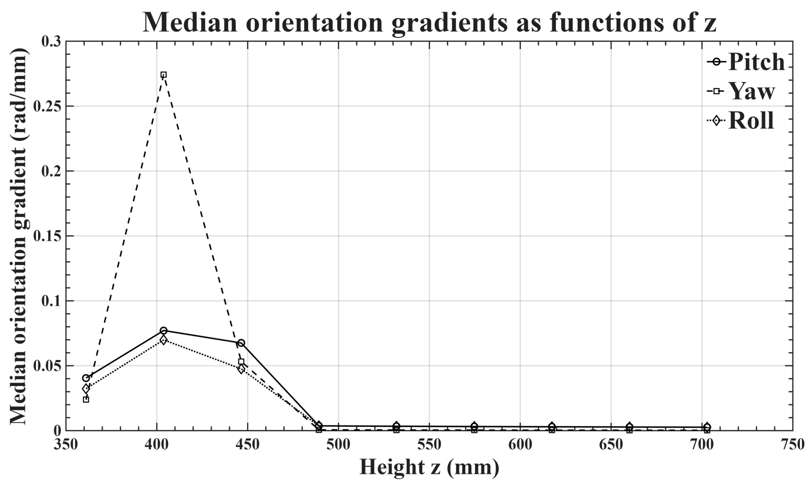

Fig. 2 Median orientation gradients across the (x,y) grid as functions of the height z.

distribution of $\|\nabla \text{pitch}\|$ across the (x,y) plane confirms that orientation variations become progressively more uniform at higher z-slices, with the lowest gradient values concentrated in the central workspace region.

Kinematic conditioning is evaluated using the translational Jacobian block J_t. Figure 4 shows the stacked z-slices colored by $\log_{10}(\kappa(J_t))$.

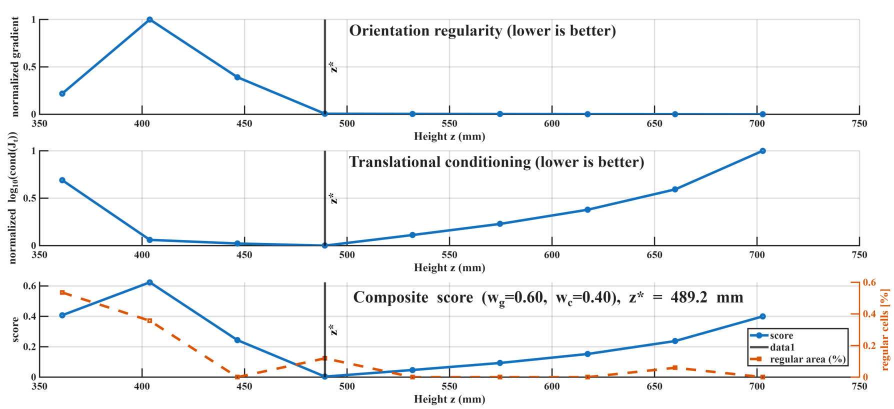

Fig. 3 Operating-plane selection through the composite score $S(z)$.

Fig. 3 shows the normalized metrics and the resulting score across the analyzed slices.The slice at $z^* = 489.2$ mm achieves the lowest composite score while pre-

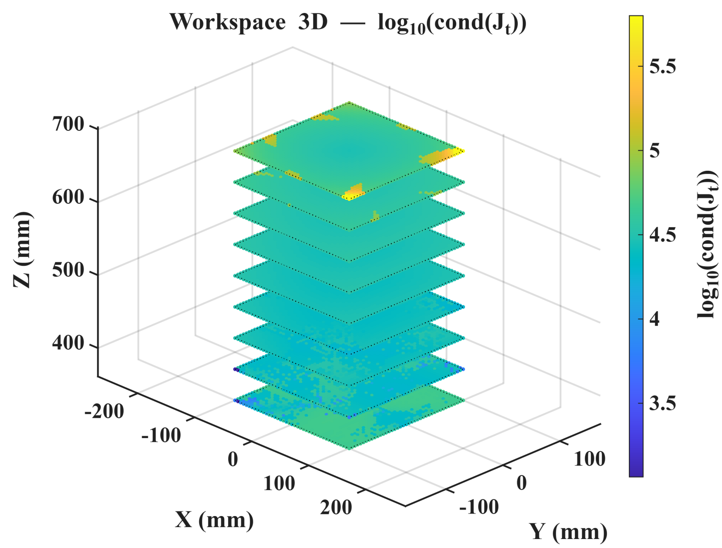

Fig. 4 Stacked representation of the sampled workspace slices colored by $\log_{10}(\kappa(J_t))$.

Table 1 Composite score $S(z)$ and regularity for the three best-performing slices.

z (mm)	Score $S(z)$	Regularity (%)
489.2	0.00351	11.9
531.9	0.04710	0.0
574.6	0.09332	0.0

Table 2 Effect of target gradients G_{target} on operating plane selection.

G_{target} (rad/mm)	R_{eq} (mm)	z^* (mm)
0.0017	600	489.2
0.0167	60	489.2
0.167	6	403.8

serving a nonzero regular region, providing the best compromise between kinematic conditioning and smooth orientation variations for probe-like motions, and is therefore selected as the operating plane (Table 1). The operating plane z^* identifies the configuration of most favorable kinematic behavior, independently of ergonomic constraints. Robustness with respect to task assumptions was evaluated by varying the target gradient G_{target}. As reported in Table 2, the selected operating plane remains unchanged for gradients corresponding to typical anatomical curvatures, shifting only for the largest tested value ($G_{\text{target}} = 0.167$ rad/mm).

4 Conclusions and Future Work

This work presented a compatibility-based kinematic framework for identifying a task-dependent operating plane z^* for a 3-RSR parallel mechanism used as a teleoperation leader interface. The proposed method combines translational Jacobian conditioning and orientation regularity into a unified metric. This enables identifying configurations with smooth probe-like motions and well-conditioned kinematics. The identified plane z^* defines the recommended initial configuration of the leader interface at the onset of the teleoperation session, ensuring desirable kinematic performance from the beginning of the probe-like motion execution. The results show that the selected operating plane offers suitable kinematic conditions for teleoperation tasks, while the selection criterion remains robust to variations in the task-dependent target gradient. The present study is limited to kinematic aspects and does not address dynamics, force transmission, or experimental validation. Future work will extend the framework toward cine-static design optimization and experimental validation on a clinical teleultrasound setup.

Acknowledgements This work has been supported by Innovation Program and FIT FOR MEDICAL ROBOTICS PNC0000007, CUP B53C22006960001, CALL 400.14 NANOTEC PNRR.

References

1. Boanta, C., Csiszar, A.: Optimal design of a parallel structure used as a haptic Interface. Mechanism and Machine Theory **116**, 69–88 (2017). DOI 10.1016/j.mechmachtheory.2017.05.013
2. Britton, N., Miller, M.A., Safadi, S., Siegel, A., Levine, A.R., McCurdy, M.T.: Tele-ultrasound in resource-limited settings: A systematic review. Frontiers in Public Health **7**, 244 (2019)
3. Carricato, M., Parenti-Castelli, V.: A family of 3-dof translational parallel manipulators. ASME Journal of Mechanical Design **125**(3), 302–307 (2003). DOI 10.1115/1.1563635
4. Gregorio, R.D.: Inverse position analysis, workspace determination and position synthesis of parallel manipulators with 3-rsr topology. Robotica **21**(6), 627–632 (2003)
5. Gritsenko, K.: Singularity analysis and workspace optimization of parallel manipulators. In: Proc. 2025 Int. Conf. on Industrial Engineering, Applications and Manufacturing (ICIEAM), pp. 627–631. Sochi, Russian Federation (2025). DOI 10.1109/ICIEAM65163.2025.11028376
6. Jiang, B., Kong, L., Zhu, S., Fang, H., Huang, G., Gu, J.: Workspace analysis of a novel 5-sps-upu parallel robot manipulator. In: Proc. 2022 IEEE Int. Conf. on Robotics and Biomimetics (ROBIO), pp. 639–643. Jinghong, China (2022). DOI 10.1109/ROBIO55434.2022.10011949
7. Kong, X., Gosselin, C.M.: Type synthesis of linear translational parallel manipulators. In: J. Lenari, F. Thomas (eds.) Advances in Robot Kinematics, pp. 453–462. Springer, Dordrecht, The Netherlands (2002)
8. Leonardis, D., Solazzi, M., Bortone, I., Frisoli, A.: A 3-rsr haptic wearable device for rendering fingertip contact forces. IEEE Transactions on Haptics **10**(3), 305–316 (2017). DOI 10.1109/TOH.2016.2640291
9. Meng, Z., Bi, J., Ding, H.: A new method for the complete workspace representation of six-degree-of-freedom parallel manipulators. In: Proc. 2022 IEEE Int. Conf. on Robotics and Biomimetics (ROBIO), pp. 1551–1555. Jinghong, China (2022). DOI 10.1109/ROBIO55434.2022.10011880
10. Merlet, J.P.: Parallel Robots. Springer, Dordrecht, The Netherlands (2000)
11. Najafi, F., Sepehri, N.: A robotic wrist for remote ultrasound imaging. Mechanism and Machine Theory **46**, 1153–1170 (2011)
12. Nigatu, H., Kim, D.: Workspace optimization of 1t2r parallel manipulators with a dimensionally homogeneous constraint-embedded jacobian. Mechanism and Machine Theory **188**, 105,391 (2023). DOI 10.1016/j.mechmachtheory.2023.105391
13. Recker, F., Höhne, E., Damjanovic, D., Schäfer, V.S.: Ultrasound in telemedicine: A brief overview. Applied Sciences **12**(3), 958 (2022)
14. Storto, E., Solazzi, M., Meola, M., Frisoli, A., Porcini, F.: Teleoperation Architectures For Remote Ultrasound Diagnostic Imaging: A Systematic Review. IEEE Trans. Biomed. Eng. pp. 1–23 (2025). DOI 10.1109/TBME.2025.3628169

15. Vu, M.H., Na, U.J.: A New 6-DOF Haptic Device for Teleoperation of 6-DOF Serial Robots. IEEE Trans. Instrum. Meas. **60**(11), 3510–3523 (2011). DOI 10.1109/TIM.2011.2164285
16. Zargarbashi, S.H.H., Khan, W., Angeles, J.: The jacobian condition number as a dexterity index in 6r machining robots. Robotics and Computer-Integrated Manufacturing **28**(6), 694–699 (2012)